The Nature of Pointer States and Their Role in Macroscopic Quantum Coherence

Philip Turner * and Laurent Nottale

Posted Date: 5 July 2023

doi: 10.20944/preprints202307.0325.v1

Keywords: quantum decoherence, macroscopic quantum mechanics, high temperature superconductivity, quantum biology

Article

The Nature of Pointer States and Their Role in Macroscopic Quantum Coherence

Philip Turner [1,*] and Laurent Nottale [2]

[1] 69 Hercules Road, Plymouth, PL9 8FA, United Kingdom
[2] CNRS, LUTH, Observatoire de Paris-Meudon, 5 Place Janssen, 92190, Meudon, France; laurent.nottale@obspm.fr
* Correspondence: p.turner.physics@outlook.com

Abstract: We consider new insights into the origin and nature of pointer states and their role in wave function collapse in macroscopic quantum coherence. The work includes new theory of quantum coherence underpinned by turbulence, generated by a field of pointer states in the form of recirculating vortices (toroids), interconnected via a vortex cascade. Decoherence occurs when the interconnected field of vortices between pointer states is disrupted by external forces, leading to their localisation. The applicability of this work is considered in addressing unresolved questions in high temperature superconductivity and macroscopic quantum processes in biological systems. We also consider its implications for our understanding of intrinsic spin and pointer states within the standard "point source" representation of a quantum particle, which intuitively requires a more complexed description.

Keywords: quantum decoherence; macroscopic quantum mechanics; high temperature superconductivity; quantum biology

1. Introduction

1.1. The general principles underpinning decoherence in quantum system

A well established mathematical framework exists to describe the outcome of experiment in quantum mechanics (QM) with high levels of precision. However, a number of questions remain relating to the fundamental physical processes that define a quantum system. Building on a body of earlier work [1–6], we consider new insights into the processes that underpin quantum coherence and wave function collapse. Through this process we shed new light on a number of inter-related postulates that underlie the present axiomatic foundation of QM [7]. Explicit examples include the complex state function, Born's postulate, the spin-statistic theorem and the Pauli exclusion principle.

1.1.2. Competing forces in diffusive and quantum systems

As described in [4], a diffusive system of environmental fluctuations that leads to collapse of a wavefunction can be written in the form of a Euler equation (Eq 1), in which D represents a standard diffusion coefficient, with the force expressed in terms of probability density P

$$\left(\frac{\partial}{\partial t} + V.\nabla\right) V = -2D^2 \nabla \left(\frac{\Delta\sqrt{P}}{\sqrt{P}}\right). \tag{1}$$

Comparing this with the quantum equivalent in the free case [8].

$$\left(\frac{\partial}{\partial t} + V.\nabla\right) V = +2\widetilde{D}^2 \nabla \left(\frac{\Delta\sqrt{P}}{\sqrt{P}}\right), \tag{2}$$

we see an equivalence between a standard fluid subjected to a force field and a diffusion process with the force expressed in terms of the probability density at each point and instant.

Preprints (www.preprints.org) | NOT PEER-REVIEWED | Posted: 5 July 2023 doi:10.20944/preprints202307.0325.v1

The "diffusion force" derives from an external potential

$$\phi_{\text{diff}} = +2D^2\Delta\sqrt{P}/\sqrt{P}. \tag{3}$$

which introduces a square root of probability in the description of a classical diffusion process, whilst the quantum force is the exact opposite, derived from an internally generated "quantum potential",

$$Q/m = -2\widetilde{D}^2\Delta\sqrt{P}/\sqrt{P}. \tag{4}$$

This interpretation offers an insight into quantum decoherence in both standard QM and macroscopic quantum systems such as High Temperature Super Conductivity (HTSC) [1]. At both scales the two forms of potential energy exist and compete in quantum systems, summarised by the total System-Environment Hamiltonians (H_S-H_E), and their interaction (H_{int})

$$H = H_S + H_E + H_{int}. \tag{5}$$

When the diffusive potential (Eq 3) exceeds the internal quantum potential (Eq 4), it leads to wave function collapse. This fits well with decoherence theory in "quantum Brownian motion", where during the decoherence process, the time evolution of position-space and momentum-space is reflected in the superposition's of two Gaussian wave packets [9]. Interference between the two wave packets is represented by oscillations between the direct peaks. Interaction with the environment ϕ_{diff} damps these oscillations leading to the emergence of "pointer states", which are minimum-uncertainty Gaussians (coherent states), well-localized in both position and momentum, thus approximating to classical points in phase space [9–15]. However, the origin and nature of "pointer states" and how they fit within the description of a wave function remains an open question.

1.1.3. The origin of pointer states and their role in decoherence

Within the theoretical framework of scale relativity, a coherent wave packet is underpinned by a fractal velocity field [1,3,17]. Whilst the concept of pointer states is highlighted, it was not dealt with in detail in this earlier work. However, it seems intuitive that pointer states equate with a fundamental "root structure", which represents a ubiquitous characteristic of fractal networks. This implies that the emergence of pointer states during wave function collapse somehow equates with the collapse of a fractal velocity field to a more robust root structure, which resists environmental interaction and accounts for the transition from a quantum to a classical description.

To clarify what this means in practice, we begin with a brief review of macroscopic quantum phenomena observed in High Temperature Superconductivity (HTSC), biological systems, superfluid helium and fully developed turbulence. From these examples we consider a number of insights which support a new description of pointer states and their role in decoherence in quantum systems.

2.0. A review of macroscopic quantum phenomena.

2.1. High Temperature Superconductivity: the role of fractal networks in the emergence of a coherent state.

In a lattice of the *p*-type cuprates, collective excitations of the electron spin structure leads to spin waves (magnons), which play a key role in forming a super conducting fluid [1]. However, the coupling mechanism that underpins the formation of an electron pair (e-pair) has not yet been fully described.

In what follows, we build on the foundations of earlier work to construct a more detailed description of e-pair coupling, which fills an important gap in our understanding of superconductvity in HTSC materials.

We begin with a review of factors reported in [1], which contribute to the emergence of macroscopic quantum coherence. Key to this is the incorporation of charged dopants within the

Preprints (www.preprints.org) | NOT PEER-REVIEWED | Posted: 5 July 2023 doi:10.20944/preprints202307.0325.v1

structure. To summarise their role, we denote ψ_n the wave function of all doping charges, whilst ψ_s represents the fraction of mobile e-pairs ($\approx$ 20 %), which form a superconducting fluid and ψ_d represents the fraction of charges which do not participate in superconductivity, i.e.

$$\psi_n = \sum_{n=1}^{N} \psi_{s_n} + \sum_{n=1}^{N} \psi_{d_n}. \tag{6}$$

During the annealing stage in the manufacture of the cuprates, charged dopants ψ_d diffuse in a thermodynamically driven process to create a disordered network across the cuprate lattice [1].

At low levels of doping, repulsive forces (coulomb interactions) between dopants are minimal. However, as dopant density (which equates with charge density ρ) increases, random fluctuations lead to increasing interactions between dopants. Beyond a critical charge density, dopants will begin to cluster, creating attractive $\mathring{A}$-scale potential well's, with the capability to harbour one or more electron-pairs. Simple models described in [1] show that this can occur in the case of 4 or more dopants with a range of possible "well configurations". An example involving eight dopants is given in Figure 1a, along with its computed quantum potential (Figure 1b).

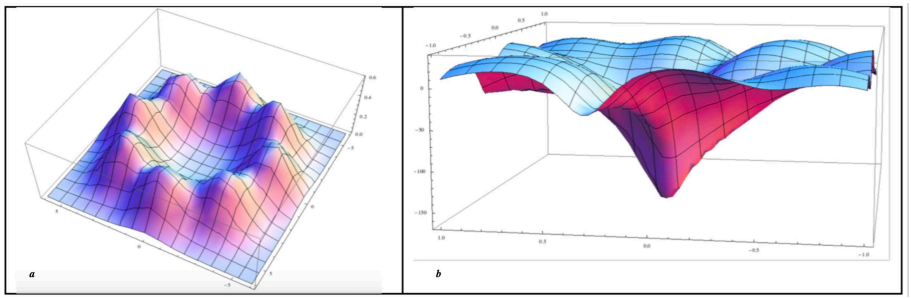

Figure 1. Reproduced from [1]. (**a**) A model of dopant density distribution, with 8 dopant sites surrounding a void zone. (**b**) A quantum potential well computed from the dopant density distribution, which can trap (localise) one or more electron pairs.

At this scale, a small cluster of charges can be seen as a quantum fluid

$$\psi_d = \sum_{n=1}^{N} \psi_d \tag{7}$$

which is expected to be the solution of a Schrödinger equation

$$\frac{\hbar^2}{2m}\Delta\psi_d + i\hbar\frac{\partial\psi_d}{\partial t} = \phi\ \psi_d, \tag{8}$$

where ϕ represents an external potential.

Introducing ρ and phase, defined as a dimensioned action A of the wave function $\psi_d = \sqrt{\rho_d} \times e^{iA_d/\hbar}$ along with the velocity field of the quantum fluid (d), given by $V_d = (\hbar/m)\nabla A_d/\hbar$, we can rewrite the Schrödinger equation in equivalent form as Euler (Eq.9) and continuity equations (Eq.10), which reflect the real and imaginary part of the Schrödinger equation,

$$\frac{\partial V_d}{\partial t} + V_d.\nabla V_d = -\frac{\nabla\phi}{m} - \frac{\nabla Q_d}{m}, \tag{9}$$

$$\frac{\partial\rho_d}{\partial t} + \mathrm{div}(\rho_d V_d) = 0, \tag{10}$$

where Q_d represents a localized quantum potential,

$$Q_d = -\frac{\hbar^2}{2m}\frac{\Delta\sqrt{\rho_d}}{\sqrt{\rho_d}}, \tag{11}$$

Preprints (www.preprints.org) | NOT PEER-REVIEWED | Posted: 5 July 2023 doi:10.20944/preprints202307.0325.v1

which is implicit in the Schrödinger equation (Eq. 8), but now explicit in the Euler equation (Eq. 9).

Whilst a superconductive fluid is expected to lie preferentially in such a well, connectivity between adjacent wells is required to support macroscopic quantum coherence and superconductivity (SC) [1]. A hint at a potential mechanism is illustrated in a second, more random assembly of 8 dopants in Figure 2A. The geometry of it's corresponding potential well (Figure 2B) reveals three open channels radiating from a central point. The probability of forming such a structure increases with increasing ρ.

At larger scale, the interaction of a randomised distribution of individual dopants (at a critical point), leads to a charge-induced fractal network of interconnected channels of the kind illustrated in Figure 3.

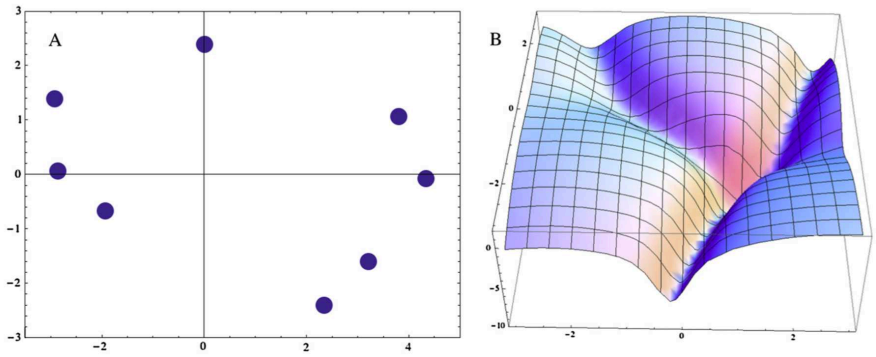

Figure 2. Reproduced from [1]. (A) A more random assembly of 8 dopant sites. (B) A quantum potential well, calculated from the distribution of the eight dopants, in which three open channels emerge to support an interconnected network at a larger scale.

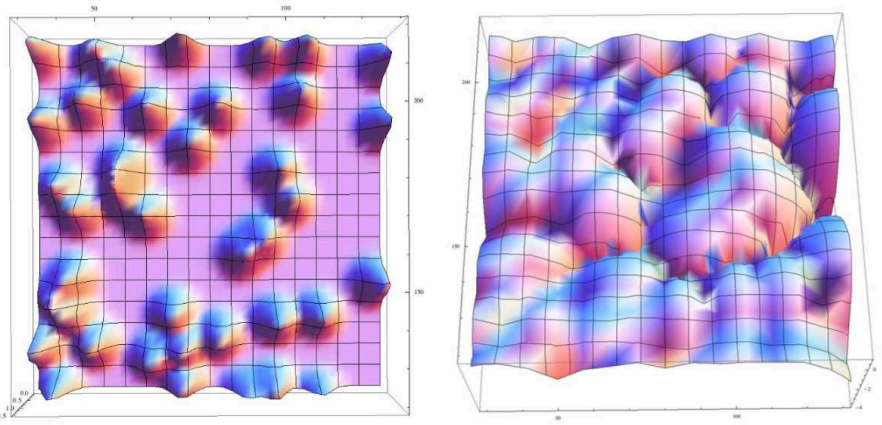

Figure 3. Reproduced from [2]. A disordered distribution of individual charges (left). The interaction of quantum potentials associated with each charge, collectively create a fractal network of hills and valleys (right).

When the fractal network reaches a "percolation threshold" (q_c), previously localised quantum potentials such as Figure 1b begin to merge with the network. The change reflects a transition from a collection of localised charges $\psi_d = \sqrt{\rho_d} \times e^{iA_d/\hbar}$ (where A_d is a microscopic action), into a charge-induced fractal network, which takes the form of a macroscopic wave function ψ_D,

$$\sum_{n=1}^{N} \psi_d \rightarrow \psi_D = \sqrt{\rho_D} \times e^{iA_D/2\tilde{D}}, \tag{12}$$

Preprints (www.preprints.org) | NOT PEER-REVIEWED | Posted: 5 July 2023 doi:10.20944/preprints202307.0325.v1

where A_D is a macroscopic action, Q_D (Eq 13) is ψ_D's associated macroscopic quantum potential (MQP) and $\hbar$ is substituted with a macroscopic parameter $\widetilde{D}$, which characterizes the amplitude and correlation length of fractal fluctuations across the MQP. The net effect is a system specific, macroscopic de Broglie scale $\lambda_{deB} = 2\widetilde{D}/v$. In standard QM, $\hbar = 2m\widetilde{D}$ [1,2].

$$Q_D = -2\widetilde{D}^2 \frac{\Delta\sqrt{\rho_D}}{\sqrt{\rho_D}}. \tag{13}$$

At the onset of the SC phase at q_c, ψ_s transforms from a microscopic scale $\psi_s = \sqrt{\rho_s} \times e^{iA_s/\hbar}$ (where A_s is a microscopic action), to a macroscopic scale, i.e.

$$\sum_{n=1}^{N} \psi_s \rightarrow \psi_S = \sqrt{\rho_S} \times e^{iA_S/2\widetilde{D}}, \tag{14}$$

where A_S is a macroscopic action, framed by the charge induced scaffold ψ_D and its associated fractal network Q_D.

During the formation of this fractal network, bosonic quasiparticles (e.g., magnons and phonons) may initially be present at a range of frequencies. However, at q_c, destructive interference effects cancel out most frequencies, leaving a coherent resonant frequency, in a process, analogous with coherent random lasing [1], which is discussed in more detail in Section 5. Evidence suggests that magnons (mg), rather than phonons, play the dominant role in e-pair coupling [1].

As doping increases beyond q_c, equilibrium between dopant repulsion and the thermodynamic drive to fractal organisation of the charges is reached, which correlates with a peak in T_c (optimal doping). Up to this point, wells, which constitute the PG phase ψ_{pg} remain localised. However, at optimum doping, ψ_{pg} merges with ψ_S, creating a single macroscopic condensate ψ_C

$$\psi_C = \sqrt{\rho_C} \times e^{iA_C/2\widetilde{D}}. \tag{15}$$

To clarify the different contributions to ψ_C, we first separate the different components.

$$\widetilde{D}^2\Delta\psi_C + i\widetilde{D}\frac{\partial\psi_C}{\partial t} - \phi\,\psi_C = -\widetilde{D}^2\Delta\psi_{MG} - i\widetilde{D}\frac{\partial\psi_{MG}}{\partial t} + \phi\,\psi_{MG} - \widetilde{D}^2\Delta\psi_S - i\widetilde{D}\frac{\partial\psi_S}{\partial t} + \phi\,\psi_S - \widetilde{D}^2\Delta\psi_D - i\widetilde{D}\frac{\partial\psi_D}{\partial t} + \phi\,\psi_D, \tag{16}$$

which when written in terms of a Euler and continuity equation reveals the four quantum potentials (Q_C, Q_{MG}, Q_S and Q_D)

$$\frac{\partial V_C}{\partial t} + V_C.\nabla V_C = -\frac{\nabla\phi}{m} - \frac{\nabla Q_C}{m} - \left(\frac{\partial V_{MG}}{\partial t} + V_{MG}.\nabla V_{MG} + \frac{\nabla Q_{MG}}{m}\right) - \left(\frac{\partial V_S}{\partial t} + V_S.\nabla V_S + \frac{\nabla Q_S}{m}\right) - \left(\frac{\partial V_D}{\partial t} + V_D.\nabla V_D + \frac{\nabla Q_D}{m}\right) \tag{17}$$

$$\frac{\partial\rho_C}{\partial t} + \mathrm{div}(\rho_C V_C) = -\frac{\partial\rho_{MG}}{\partial t} - \mathrm{div}(\rho_{MG}V_{MG}) - \frac{\partial\rho_S}{\partial t} - \mathrm{div}(\rho_S V_{2e}) - \frac{\partial\rho_D}{\partial t} - \mathrm{div}(\rho_D V_D). \tag{18}$$

Whilst ψ_D remains static, in analogy with Eq's (9 & 10), it plays a key, but indirect role as a fractal electromagnetic scaffold, acting as an exterior potential (Q_D), within which spin-waves ψ_{mg} merge to form a macroscopic bosonic condensate ψ_{MG},

$$\sum_{n=1}^{N} \psi_{mg} \rightarrow \psi_{MG} = \sqrt{\rho_S} \times e^{iA_S/2\widetilde{D}}. \tag{19}$$

Preprints (www.preprints.org) | NOT PEER-REVIEWED | Posted: 5 July 2023 doi:10.20944/preprints202307.0325.v1

As initially proposed in [1], on re-integration under the form of a macroscopic Schrödinger equation, the exterior macroscopic quantum potentials Q_D and Q_{MG} become explicit, whilst Q_d, present as an exterior potential in the microscopic equation Eq.8, disappears as it becomes internalized as part of Q_D at the macroscopic scale. This allows a simplification of Eq.16 to

$$\widetilde{D}^2\Delta\psi_C + i\widetilde{D}\frac{\partial\psi_C}{\partial t} - \left(\frac{\phi + Q_D + Q_{MG}}{2}\right)\psi_C = 0. \tag{20}$$

However, we also proposed a second interpretation in which ψ_{MG} and its associated quan- tum potential Q_{MG} might play a more dynamic, integral part of the conducting fluid ψ_C. In this scenario ψ_{MG} and Q_{MG} would become absorbed into ψ_C and Eq.20 becomes

$$\widetilde{D}^2\Delta\psi_C + i\widetilde{D}\frac{\partial\psi_C}{\partial t} - \left(\frac{\phi + Q_D}{2}\right)\psi_C = 0. \tag{21}$$

To clarify which of these two interpretations is correct, we need to determine the precise role of magnons in the e-pairing mechanism. In addition we revisit two unresolved questions, including:

- Why T_c is significantly higher in HTSC materials, compared with conventional SC materials.
- Why are critical temperatures in the pseudo gap ψ_{PG} significantly higher than in the super conducting fluid ψ_S.

We consider these questions alongside a proposed new mechanism to account for the role of ψ_{MG} as an internal potential (implicit in Eq.21), which is fundamental to the coupling of e-pairs and ψ_C. Before addressing these issues (in Section 5), we consider a number of additional factors, which contribute to the construction of a more detailed picture of the underlying mechanisms at play.

As a final point, originally made in [1], we note that as doping increases beyond an optimum level associated with maximum T_c, dopant packing density increases to a point where we see the emergence of a more homogenous dopant lattice structure. Under these conditions, the charge induced fractal network which underpins quantum coherence declines, leading to a decline in the strength of fractal spin wave fluctuations ψ_{MG} and coupled e-pairs. At this second quantum critical point, the SC properties of the material disappear.

2.2. Macroscopic quantum behaviour in biological structures.

On first sight HTSC and biological systems appear to have little in common. However, recent studies [1–4] have identified a number of shared macroscopic quantum processes, which have the potential to explain the emergence of a range of structures and processes typically associated with living organisms.

We illustrate the concept with a summary of work on biomimetic structures grown from $BaCO_3 - SiO_2$ solutions [3,4], where sources of "charge" included protons (from atmospheric CO_2) and charged biomolecules, in the form of gibberellic acid (GA) and cytokinin (CK).

At a molecular scale the emergence of structure in biological systems is strongly influenced by quantum vacuum and thermal fluctuations (collectively "environmental fluctuations") which act as a sea of harmonic oscillators. A combination of "environmental fluctuations" and levels of ionisation (which dictate charge density ρ), have a fundamental impact on the trajectory and dynamics of particles as they interact to form larger structures. The principle is illustrated in Figure 4a, where $\rho \to 0$ in an inert gas environment. In this scenario $BaCO_3 - SiO_2$ assembly, unhindered by repulsive charges (normally generated by protons from atmospheric CO_2), led to the growth of a crystal lattice.

By contrast, as ρ increases, repulsive forces between adjacent charged particles create a barrier to bonding, facilitating greater particle interaction with environmental fluctuations. The implications of this are illustrated in Figure 4b, where we see successive solutions during the evolution of a time-dependent Schrödinger equation in a 2D harmonic oscillator potential, which leads to a model of bifurcation at a molecular scale. The jump from a one-body to a two-body branched structure occurs

Preprints (www.preprints.org) | NOT PEER-REVIEWED | Posted: 5 July 2023 doi:10.20944/preprints202307.0325.v1

as the energy level increases from a fundamental level ($n = 0$) to the first excited level ($n = 1$). An iterative bifurcation process leads to a branched molecular assembly, high levels of disorder and a fractal charge density distribution.

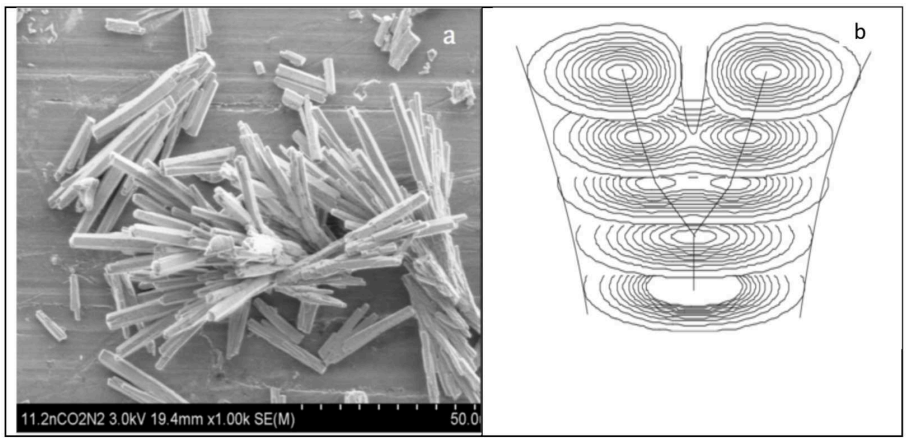

Figure 4. (a) A $BaCO_3 - SiO_2$ crystalline lattice structure, reproduced from [3]. (b). A model of bifurcation, described by successive solutions of the time-dependent 2D Schrödinger equation in an harmonic oscillator potential plotted as isodensities, reproduced from [**?**].

As with discussions on HTSC in Section 2.1, as the charge induced fractal network increases beyond a percolation threshold q_c, the interaction of quantum potentials associated with individual charges creates a fractal network of interconnected channels. This can be seen as analogous with that illustrated in Figure 3, but now in 3D, that can support the emergence of a bosonic condensate, which underpins the emergence of different structures [3,4].

To illustrate this principle we consider structures grown from $BaCO_3 - SiO_2$ solutions, with ρ being dictated by protons, released through dissolution of atmospheric CO_2. Figure 5a illustrates a fern-like (fractal leaf) structure, which reflects partial decoherence of a macroscopic wave function [3]. Despite its relatively low fractal dimension (D_F), it still exhibits a component of long range order, its D_F being determined by the strength of a residual field (Q_D) and associated fractal fluctuations $\widetilde{D}$, relative to external diffusive forces. As ρ increases further, we see a change in packing of dendritic nm-scale fibrils, with an increase in D_F leading to a more classic leaf-like form illustrated in Figure 5b.

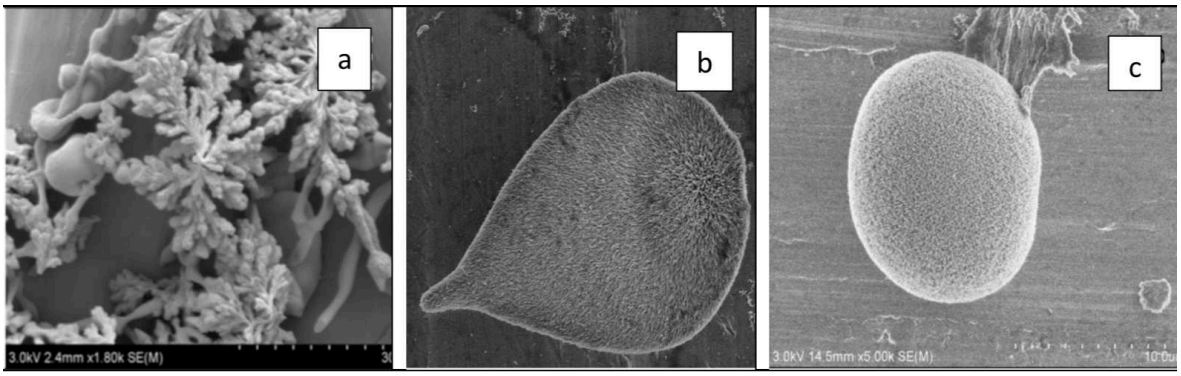

Figure 5. (a) A fractal leaf-like structure. (b). A standard leaf structure. (c). A cell-like structure.

As illustrated in Figure 5c, a further increase in ρ, through the incorporation of GA as an additional source of charge in the $BaCO_3 - SiO_2$ system, led to a spherical, non-differentiated stem cell-like structure of $\approx 15\,\mu m$ diameter. The structure is composed of densely packed ($\approx 5\,nm$ diameter) dendrites, grown symmetrically from a centre to fill the space via an iterative process of bifurcation.

Preprints (www.preprints.org) | NOT PEER-REVIEWED | Posted: 5 July 2023 doi:10.20944/preprints202307.0325.v1

The structure closely resembles a real cell (without a cell wall) with $BaCl_2 - Na_2SiO_3$/GA composite dendrites replicating the dendritic structures formed by microtubules and actin filaments, which dominate the cytoplasm where most cellular activities, including cell division occur [4].

The hypothesis that this cell-like structure is underpinned by a macroscopic quantum wave function is illustrated in Figure 6a, which reveals a collection of structures comparable to the single cell in Figure 5c. Some structures are captured in what looks like a process of division. This is confirmed in Figure 6b, which captures the transition from a one-body to a two-body structure.

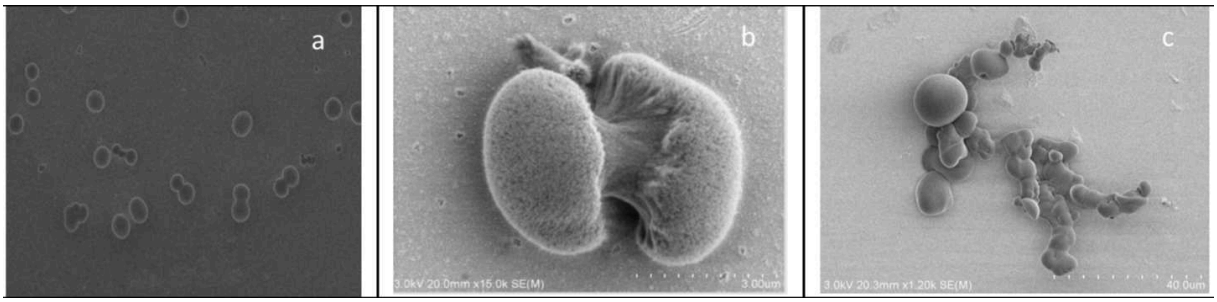

Figure 6. (a). A monoculture of spherical structures with evidence of a division process. **(b).** The process of cell division. In order to grow beyond a critical point, a symmetric one-body structure, composed of a fractal fluid of molecular trajectories becomes unstable and is forced to divide. Here frozen in time, we see an unstable intermediate step in the dynamic transition from a one-body to a two-body structure. **(c.)** A branched multicellular structure.

We identify the process which underpins the cell division process captured in Figure 6b with an earlier theoretical description [3,4,8,16,17]. The process, summarised in Figure 7a, reveals stationary solutions of a time-dependent Schrödinger equation in a 3D harmonic oscillator potential, whilst Figure 7b, reveals successive figures, giving the isovalues of the density of probability for 16 time steps. The first and last steps ($1, n = 0$ and $16, n = 1$) are solutions of the stationary (time-independent) Schrödinger equation, whilst intermediate steps are exact solutions of the time-dependent Schrödinger equation reflecting transient structures. Figure 7b shares a number of common features with the bifurcation process in Figure 4b, the key difference being that in the case of bifurcation, the previous structures remain and add to themselves instead of disappearing as in cell division. The only other difference lies in the quantum of action, with Figure 4b being based on $\hbar$ rather than a macroscopic constant in Figure 7b, although the bifurcation process (Figure 4b) is also valid for a macroscopic quantum system at both sub-cellular and multicellular scales.

Like Figure 7a, Figure 6b reflects a point-like probability density. However, it also reveals that division is supported by a single, interconnected system of coherent fluctuations, in which at each point in the initial one-body system, trajectories exist that connect the two-body structures.

Preprints (www.preprints.org) | NOT PEER-REVIEWED | Posted: 5 July 2023 doi:10.20944/preprints202307.0325.v1

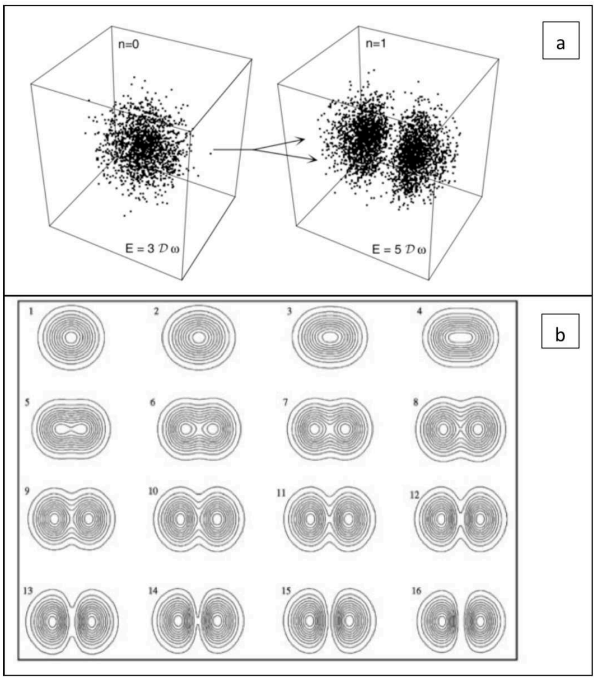

Figure 7. Reproduced from [4]. (a). A generic model of division, (b). Model of cell division.

It appears that the cell division is underpinned by a macroscopic quantum process with an increase in energy, associated with higher levels of quantisation, being linked to increasing ρ [4]. This is supported by Figure 6c, where a further increase in ρ leads to branched multicellular structure, which bears a striking resemblance to early stem cell division in *Arabidopsis thaliana* reported in [4].

Alongside charge density, bifurcation processes, driven by environmental fluctuations are fundamental to the emergence of the fractal architecture required to determine whether a macroscopic quantum system emerges. Depending on conditions, the process of bifurcation can repeat itself over a broad range of scales, to create a range of structures, from proteins to cell organelles and cell walls, which constitute a living cell. The cell as the "quanta of life", then has the potential to repeat the process, creating new networks and levels of organisation, through spontaneous duplication and bifurcation.

The fractal dimension of a multicellular structure is dictated by charge density and its spatial distribution. Depending on the average charge on each cell and the level of interaction with the environment (external to the system under consideration), we see the emergence of a diverse range of cellular and multicellular structures [3,4].

One of the experimental phenomena reported in [4], of particular interest when considering intrinsic spin in quantum systems, relates to the emergence of spiral structures (e.g. Figure 8a) at higher levels of charge density generated using CK. These structures share features comparable to structures in single-celled spiral diatoms such as *Chaetoceros debilis* and multicellular organisms such as *Arapidopsis thaliana*, where spiral thickening occurs in tracheary elements [4].

Preprints (www.preprints.org) | NOT PEER-REVIEWED | Posted: 5 July 2023 doi:10.20944/preprints202307.0325.v1

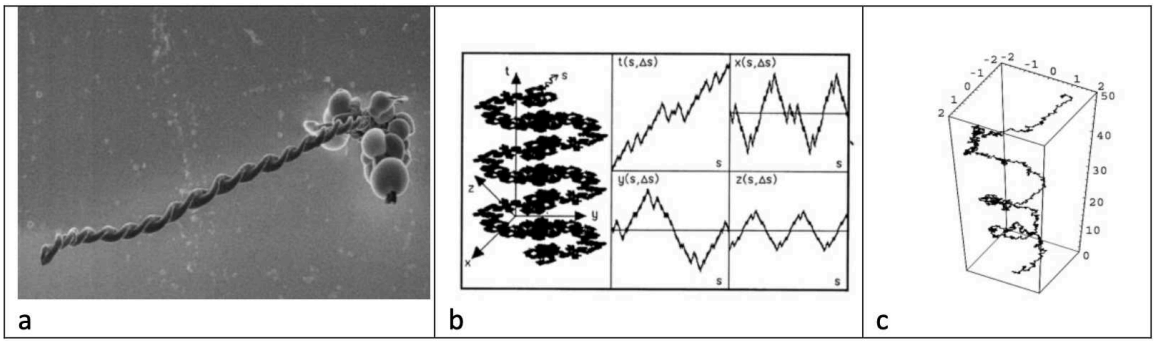

Figure 8. (a) Reproduced from [4]. Growth of continuous spiral, underpinned by a coherent bosonic field. Each stage of assembly adds to previous growth, creating an aggregated time series. (b). Schematic representation of a fractal curve in space time from [18]. The evolution of its coordinates is described by four fractal functions of the normalized curvilinear coordinate s intrinsic to the fractal curve. (c). Numerical simulation of a typical spinorial geodesic in a fractal space, reproduced from [19]. The x, y coordinates of the spiral path are quantized in units of $\hbar$.

A step towards understanding these spiral features emerges in earlier work, which modelled the emergence of a spin-like internal angular momentum in a fractal spacetime [18–20]. The Principle, illustrated in Figure 8b shows a schematic representation of the fractal path of a particle in an inertial frame of reference. The spiral path emerges as a dynamic causal structure; causal order being determined by the specific spacetime coordinates in a series of sequential events within a 4D space-time, in which all four dimensions, including the invariant proper time s, are fractal.

Both Figure 8a and 8b feature a vortex-like structure, which reflects the physical integration of consecutive slices of a fractal space. As the cell in Figure 8a grows in length, rotational forces lead to the emergence of a spiral structure, supported by a macroscopic wave front, as it evolves over time, to produce a continuous 4D fractal spacetime construct.

The helical (solenoidal) structure in Figure 8a emerges as an aggregated time series, with not just one, but a range of probable outcomes (paths) being revealed, with an average wavelength $\lambda \approx 6\mu m$ in the mid infrared range of $3 - 8\mu m$ (37-100 THz). It suggests that the force dictating the structure is underpinned by coherent thermal phonons in the mid IR range.

The phenomena offers an important insight into some recent developments in quantum biology [4]. For example, it is a small step to visualise how such a system could play a role in photosynthetic systems, offering a mechanism for translating photons into a coherent energy flux, which is transferred via coherent thermal phonons to different sites within a plant. In the case of the single celled spiral diatoms where this kind of spiral structure dominates the cell's anatomy, it could play a particularly effective role in facilitating photosynthetic processes.

The concept of spin in macroscopic quantum systems is of considerable interest, not just for biological systems, but also for what we may learn with respect to spin in standard quantum systems. We explore this further in Section 3.3, once we have completed the preliminary background work required to support new proposals.

2.3. Turbulent fluids and the link to quantum coherence.

The emergence of quantum-like forces in fractal media represents one of the founding principles of the theory of scale relativity. However, an important question remains relating to the origin of a fractal space time.

In developing the theory of scale relativity, it was suggested as early as 1993 ([18] Chap. 7) that a fractal medium could simulate, at some level, a fractal space, and that particles moving in such a medium may therefore acquire macroscopic quantum-type properties.

Preprints (www.preprints.org) | NOT PEER-REVIEWED | Posted: 5 July 2023 doi:10.20944/preprints202307.0325.v1

One of the key objectives of earlier work [1–4], was to test the hypothesis that quantum forces could emerge in fractal media, at macroscopic scales. Work on HTSC and biological systems, summarised in Sections 2.1 and 2.2, demonstrated a remarkable level of support for this hypothesis.

Taking the idea a step further, recent work [6] reveals fresh insights into the properties of turbulent systems, including the identification of a quantum signature at high levels of turbulence in "classical fluids".

The analysis in [6] involved data generated from von Karman experiments, with turbulence generated by two contra-rotative disks. During this work, pathways through the fluid were monitored with the aid of tracer particles ($<\approx 100\mu m$). Results suggest that in fully developed turbulence, (a Reynolds number $R_\lambda >\approx 500$), a cascade of eddies/vortices, collectively generate a saturated, interconnected, vortex field and the emergence of macroscopic fluctuations, which underpin what appears to be a first stage in the emergence of a macroscopic wave function, within which both classical and coherent signatures were identified. An analogy with such a system can be found in the early onset of a coherent state, described at q_c (Eq.14) in HTSC [1], where we see the emergence of a critical percolation threshold within the fractal network. Within this context, we identify the emergence of a macroscopic wave function as the sum of interconnected individual (classical) vortices (vo), leading to a vortex induced macroscopic field (VO).

$$\sum_{n=1}^{N} v_o = V_O \rightarrow \psi_{V_O} = \sqrt{\rho_{V_O}} \times e^{iA_{V_O}/2\widetilde{D}}. \tag{22}$$

where A_V is a macroscopic action and Q_v (Eq 23) is its associated MQP.

$$Q_v = -2\widetilde{D}_v^2 \frac{\Delta_v \sqrt{P_v}}{\sqrt{P_v}}, \tag{23}$$

The above discussions are based upon a 2D analogy between HTSC and turbulent systems. Figure 14 in [21] illustrates simulations of high intensity, 3D vortex network in homogeneous and isotropic turbulence reported for $R_\lambda \approx 150$. The simulation suggests that the strongest vorticity is organised in elongated thin tubes.

As a general point, vortices, in close proximity and circulating in the same direction, attract and interconnect at points along their length. This can ultimately lead to the merger of vortices to form larger vortex structures whose circulation will equal the sum of the circulations of the constituent vortices. In the simulation work in [21], there is no mention of interconnection between vortices. However, the high vortex density image (Figure 14 in their paper), suggests that this could be reasonably anticipated within a network of vortices at $R_\lambda \approx 150$. When considering vortex densities at $R_\lambda >\approx 500$, reported in [6], the probability of an interconnected vortex field $\rightarrow 1$.

The largest, most energetic vortices in a turbulent fluid dominate the space. As they interact, they generate a cascade of smaller eddies/vortices, which act as carriers of force between them. It appears intuitive that larger vortices, with the potential to facilitate transport of tracer particles, may be regarded as analogous with quantum tunnelling, whilst the less energetic component of the turbulent field reflects the classical component of the system.

The analysis raises an interesting question around the relationship between turbulent space time and the origins of quantum particles (bosons and fermions). It suggests that the origins of fractal space time, chaos and irreversibility, that sit at the heart of a coherent quantum system in scale relativity theory emerge from pure turbulence. These concepts are developed further with respect to superfluid helium in Section 2.4 and HTSC materials in Section 5.

2.4. Superfluid Helium.

The report of a quantum signature in fully developed turbulence ($R_\lambda > 500$) [6], suggests that a macroscopic quantum phenomena such as superfluid helium may be underpinned by turbulence

Preprints (www.preprints.org) | NOT PEER-REVIEWED | Posted: 5 July 2023 doi:10.20944/preprints202307.0325.v1

at microscopic scales. To explore this idea further, we consider the different processes that define a coherent state.

In the turbulent fluid scenario in Section 2.3, two contra-rotating discs generate a turbulent fluid, which can lead to partial coherence. Comparing this with superfluid helium, the turbulent fluid which underpins coherence is generated by a collection of spinning nuclei, whose magnetic flux interacts to create a Bose-Einstein Condensate (BEC). Within this system, the nuclei remain localised, whilst the magnetic flux becomes delocalised (shared between nuclei). From this description, we identify the nuclei with first order "pointer states".

We have discussed how a rotating vortex like structure naturally emerges from a fractal network as a causal dynamic structure in both classical and quantum systems, but with important differences between the two. In a classical turbulent fluid, the energy of a vortex dissipates due to fluid viscosity, so a vortex line generally ends within the fluid. We see this clearly in a recent study [22] of superfluid helium, where just above the critical transition temperature (T_c), Figure 9a reveals a chaotic distribution of localised vortices, highlighted by small, frozen tracer particles of hydrogen. The image is typical of what one might expect in a classical turbulent fluid. It confirms that not all turbulent systems result in a coherent fluid.

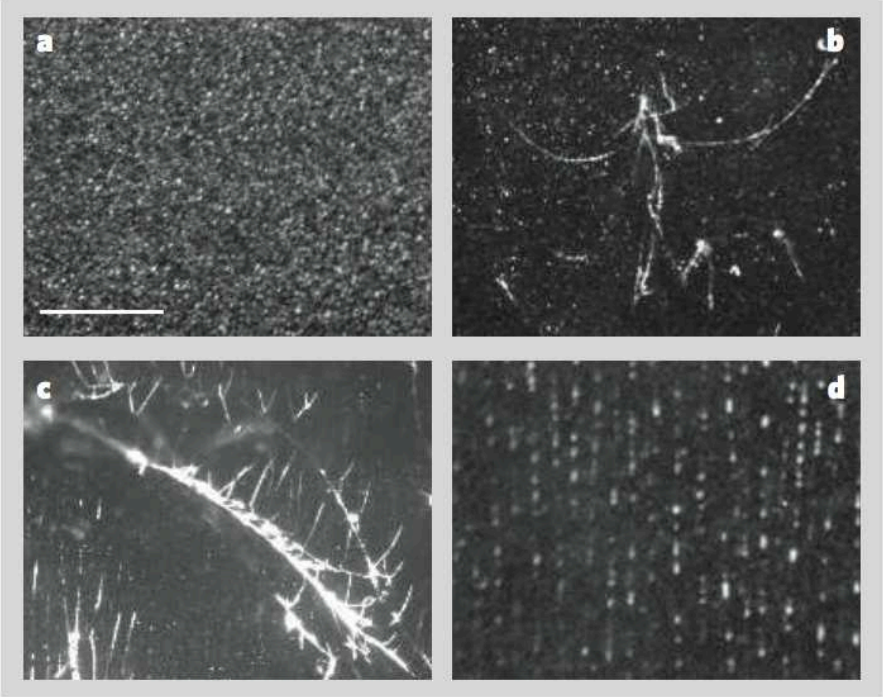

Figure 9. Quantized vortex cores in liquid helium, reproduced from [22]. Images of particles under different conditions: a, just above the transition temperature, when they are uniformly dispersed; b,c, on branching filaments just below the transition temperature; and d, regrouping along vertical lines for steady rotation about the vertical axis. Scale bar, 1mm.

Contrasting Figure 9a with the superfluid phase of helium (Figure 9b and Figure 9c), viscosity $\rightarrow 0$, so vortices propagate without resistance and exist almost indefinitely as "string-like" vortex filaments. Fluid in the form of a vortex (and matter trapped by it) transports mass, energy and momentum over considerable distances without dissipation. According to Helmholtz's second theorem, a vortex filament cannot end in a fluid; it must extend to the boundaries of the fluid or form a closed path. Whilst limited by this constraint, vortex filaments may in theory also form either an ouroboros, or bifurcate (in the case of Figure 9b and Figure 9c), leading to the emergence of an interconnected fractal

Preprints (www.preprints.org) | NOT PEER-REVIEWED | Posted: 5 July 2023 doi:10.20944/preprints202307.0325.v1

network of extended vortices. As suggested in Section 2.3, this has the potential to facilitate tunnelling in quantum systems.

Note that fewer vortices are apparent when comparing Figure 9b and 9c to Figure 9a, because light intensity was reduced to highlight the brighter filaments in the image [22]. In addition, only a small proportion of the filamentous network of vortices present in the system were recorded due to a limit on the availability of tracer particles.

The example illustrates how the emergence of quantised vortices represents a key feature of a quantum fluid such as a BEC. By implication, it is interesting to consider the occurrence of an analogous mechanism within a quanta of superfluid that takes the form of a particle in standard QM. We explore this idea further in Section 4.

A further insight from the results reported in [22], is hightlighted in Figure 9d. The figure illustrates that when a force (rotational in this case) is applied to superfluid helium, vortices align in the direction of the force applied. In an analogous way (see Section 5), one would expect vortices in a magnon condensate in HTSC media to align within an electric field and facilitate superconductivity.

3.0. A geometric interpretation of spin.

Having reviewed some useful examples of macroscopic quantum coherence, we build on this work with a more detailed consideration of the properties of quantum systems. We begin with a review of the current status of spin as generally portrayed within the context of $SU(2)$ and the Lorentz group $SO(3,1)$.

3.1.$SU(2)$

In the special unitary group $SU(2)$, the $j = 1/2$ representation in Eq.24, represents quantum mechanical spin in spin-1/2 particles as rotations in complex space,

$$J^x_{1/2} = \frac{1}{2}\begin{pmatrix} 0 & 1 \\ 1 & 0 \end{pmatrix} = \frac{\sigma^1}{2},\ J^y_{1/2} = \frac{1}{2}\begin{pmatrix} 0 & -i \\ i & 0 \end{pmatrix} = \frac{\sigma^2}{2},\ J^z_{1/2} = \frac{1}{2}\begin{pmatrix} 1 & 0 \\ 0 & -1 \end{pmatrix} = \frac{\sigma^3}{2}, \tag{24}$$

where σ^i are the Pauli Matrices. Choosing the Cartan generator $J^z_{1/2}$ as the diagonal, its eigenvectors

$$|\uparrow\rangle_z = \begin{pmatrix} 1 \\ 0 \end{pmatrix}, \quad |\downarrow\rangle_z = \begin{pmatrix} 0 \\ 1 \end{pmatrix}. \tag{25}$$

are the basis vectors upon which $SU(2)$ acts, with eigenvalues

$$J^z|\uparrow\rangle_z = +\frac{1}{2}\,|\uparrow\rangle_z,\ J^z|\downarrow\rangle_z = -\frac{1}{2}\,|\downarrow\rangle_z. \tag{26}$$

In contrast to the j=1/2 representation, particles with spin-1 are portrayed by the adjoint, $j = 1$ representation of the rotation group (Eq.27), in which only J^z_1 is diagonal, with eigenvalues $1, 0, -1$.

$$J^x_1 = \frac{1}{\sqrt{2}}\begin{pmatrix} 0 & 1 & 0 \\ 1 & 0 & 1 \\ 0 & 1 & 0 \end{pmatrix} = \tau^1,\ J^y_1 = \frac{i}{\sqrt{2}}\begin{pmatrix} 0 & -1 & 0 \\ 1 & 0 & -1 \\ 0 & 1 & 0 \end{pmatrix} = \tau^2,\ J^z_1 = \begin{pmatrix} 1 & 0 & 0 \\ 0 & 0 & 0 \\ 0 & 0 & -1 \end{pmatrix} = \tau^3. \tag{27}$$

The tau matrices τ^i represent the 3×3 analog of the Pauli matrices.

Within this "framework", intrinsic spin of a "point particle" such as an electron, is seen as a purely quantum mechanical phenomenon, generally visualised within the context of a Bloch sphere interpretation [25], in which the two spin states (S^+, S^-) reflect the two sides of a complex projective plane $\mathbb{CP}^1$.

Preprints (www.preprints.org) | NOT PEER-REVIEWED | Posted: 5 July 2023 doi:10.20944/preprints202307.0325.v1

This interpretation falls short of an intuitive description of the internal structure of a spin-1/2 particle and the concept of spin as a rotation through spacetime, analogous with $SO(3)$ in classical physics. The gap necessitates a fresh look at the underlying meaning of $SU(2)$ and additional information required to describe the structures and processes that are implicit (but not explicit) within the group.

As an emergent property of a 4D fractal space-time, intrinsic spin is supported in part by work illustrated in Figure 8c, which represents a model of a spiral fractal path of an electron, underpinned by a Pauli spinor. The figure represents just one of an infinite number of possible realisations of an electron, which collectively represent a coherent rotating "fluid" of geodesics. However, the concept of a rotating fluid does not on its own reveal the full picture.

To develop a more comprehensive description we begin with the vortex-like rotating matter wave illustrated in Figure 8a, which is underpinned by a macroscopic wave function. Whilst the structure is quantised along x and y coordinates, the axis of rotation (the z coordinate) remains open. If we compare this with an electron's vortex-like path in Figure 8c, there are some important differences.

1. As stated previously in [4], with respect to Figure 8a, only the macroscopic bosonic field (which underpins the structure as it grows along its z axis) is coherent.
2. Figure 8a represents a bundle of geodesics, whilst Figure 8c reflects just one, which suggests an incomplete representation of an electron.
3. The nature of a coherent packet of matter such as an electron, quantised along all three (x,y,z) coordinates suggests some form of closed, recirculating "fluid of geodesics" in the form of a torus, such as illustrated in (Figure 10). However, to meet a criteria that relate to $\mathbb{CP}^1$, we need to translate this into an approximation of a two-dimensional torus

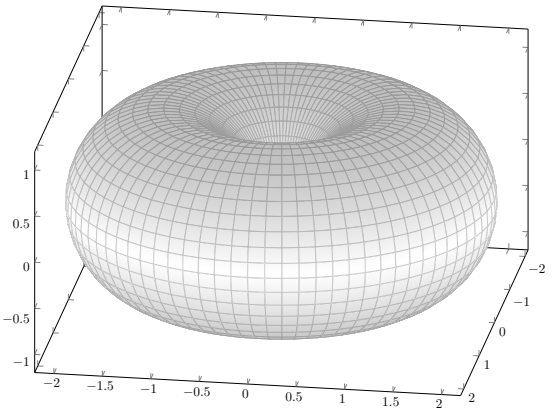

Figure 10. A torus.

Digging deeper into these issues, consider a tracer trapped within a rotating vortex analogous to that illustrated in Figure 8c. We begin with a tracer sitting in the North East (NE) quadrant of the vortex, pointing NE, then map the tracer's position and orientation as it rotates around the z axis. After a 360^o rotation it will have changed position along the z axis, but will point once again in the same direction (NE). In other words, an open vortex clearly reflects the statistical description of a $j = 1$ representation of $SU(2)$ (Eq.27), in which a spin-1 particle (a boson) requires a 360^o rotation to resume its original state.

At a simplistic level, it seems intuitive that a vortex plays the role of a boson with the capability to transfer energy, via the fabric from which it is constructed.

If we consider the emergence of vortex like structures at a larger scale, an analogous scenario can be found in a highly ionised atmosphere (or plasma), associated with an intense fire or thunderstorm,

Preprints (www.preprints.org) | NOT PEER-REVIEWED | Posted: 5 July 2023 doi:10.20944/preprints202307.0325.v1

where charge density reaches extremely high levels. At a critical point, the build up of a potential difference between different points in space creates a force and an associated "action", in the form of a rotating vortex (a tornado) as an emergent property of a charge induced fractal network. Once the difference in charge between points in space reaches equilibrium (via the action of the vortex), the vortex dissipates. This description represents a striking example of boson-like behaviour, with the vortex transferring energy from one point to another. As seen in superfluid helium (Figure 9b and 9c), it can also transport matter. This principle has important implications with respect to HTSC, which we elucidate in Section 5.

When we reflect on these new insights, we see the validation of an earlier prediction of the emergence of a macroscopic quantum potential and quantum force from an ionised fractal media such as a plasma [26]. As an example from this earlier work, numerical integration of a Euler plus continuity one-dimensional system, with generalised quantum potential, reproduced the expected motion of an quantum oscillating wave packet in an harmonic oscillator field (Figure 1). In practice, the emergence of a 3 dimensional wave packet as revealed in Figure 8a, offers an insight into how the simplified, one dimensional model in [26] translates into a 3 dimensional wave packet.

To shed light on what differentiates a spin-1 structure from a spin-1/2 particle, we contrast the spin-1 vortex scenario with a continuously recirculating fluid in the form of a torus such as Figure 10. Once again we visualise a tracer starting in the NE quadrant (of the torus), pointing NE and map its orientation relative to its position, as it travels through the structure.

After a 360^o rotation through the torus there is an equal probability that the tracer will sit in either the NE or North West (NW) quadrant. If by chance it returns to the same (NE) quadrant, it will (in all scenarios) have reoriented to face the opposite direction to which it started.

As the tracer continues its path on a second 360^o rotation through the torus, there is once again an equal probability that it will sit in the NE or NW quadrant. In the event that it returns to the original NE quadrant it will have reoriented once again, to point in the original direction (NE).

The scenario clearly describes the $j = \frac{1}{2}$ representation of $SU(2)$ (Eq.24) in which a spin-1/2 particle requires a 720^o rotation to resume its original state.

The concept of a closed vortex (toriodal) ansatz to describe a quantum particle such as an electron or proton is not new [23,24].

A number of useful insights emerge from such a description:

- When considering flow within a recirculating torus it is impossible to predict the precise position and orientation of a tracer at any specific point in time. It can only be described in terms of a probability $P \propto \psi^2$ (the Born postulate [7]) after two full rotations of the torus (which defines ψ), explaining the statistical origins of a spin-1/2 particle in standard QM.
- The double rotation through a torus gives physical meaning to the $2 \rightarrow 1$ relationship between $SU(2)$ and $SO(3)$ [25].
- A toriodal interpretation of a spin-1/2 particle resolves the problem of infinities associated with a point particle, in which angular momentum of a point mass following a classical spiral path should vanish as $r \rightarrow 0$. Instead, we can intuitively link $\hbar$ as a minimum measure of action with the rotation of a torus (or a vortex in the case of a spin-1 boson).
- If we consider a particle as a dynamic recirculating torus and c represents an upper limit on rotational velocity ($\dot{\omega}$), its rotational energy equates with the mass of a stationary particle, i.e., $e = mc^2$. It means that as a measure of action, $\hbar$ defines a lower limit on a scale at which velocity, scale and mass are unified.

these results support our understanding of the main postulates of QM in Nottale 2007

3.2. The Lorentz group $SO(1,3)$.

As the double cover of $SU(2)$, the Lorentz group $SO(1,3)$ represents transformations in flat, 4D Minkowski space, but how do we explain this in terms of relations between the Euclidean, Kronecker

Preprints (www.preprints.org) | NOT PEER-REVIEWED | Posted: 5 July 2023 doi:10.20944/preprints202307.0325.v1

delta matrix (δ_{ij}) and the Minkowski metric ($\eta_{\mu\nu}$) and how $\mathbb{CP}^1$ relates to an intuitive understanding of a quantum particle.

Having established a fermion as a recirculating torus represented by the $j = 1/2$ representation of $SU(2)$, we consider the transition to a relativistic scenario represented by $SO(1,3)$ as $\omega \to c$. If we exclude the influence of other possible factors, we can expect that in such a scenario, rotation of a particle with mass, will lead to extreme dilation of its toroidal structure along x and y coordinates with a corresponding contraction in the z coordinate. The action reflects symmetry breaking associated with a transition from a 3D torus, represented by δ_{ij}, into an approximation of a 2D torus, represented by $\eta_{\mu\nu}$ and the dot product

$$\mathbf{v}.\mathbf{v} = \eta_{\mu\nu} v^\mu v^\nu = -t^2 + x^2 + y^2 + z^2. \tag{28}$$

Whilst an event measured in different inertial reference frames may give different values (observer A sees t, x, y and z, and observer B sees t', x', y' and z'), they are still physically equivalent, i.e.,

$$-t^2 + x^2 + y^2 + z^2 = -t'^2 + x'^2 + y'^2 + z'^2, \tag{29}$$

being related through Lorentz transformations Λ (a combination of Euler transformations and Lorentz boosts), that preserve the dot product (Eq.28).

Whilst Euler transformations take the form of rotations (R) of vectors around the origin, where θ represents an angle mixing spatial dimensions,

$$\begin{aligned}
[R_x(\theta_x)]^\mu_\nu &= \begin{pmatrix} 1 & 0 & 0 & 0 \\ 0 & 1 & 0 & 0 \\ 0 & 0 & \cos\theta_x & \sin\theta_x \\ 0 & 0 & -\sin\theta_x & \cos\theta_x \end{pmatrix}, \\
[R_y(\theta_y)]^\mu_\nu &= \begin{pmatrix} 1 & 0 & 0 & 0 \\ 0 & \cos\theta_y & 0 & -\sin\theta_y \\ 0 & 0 & 1 & 0 \\ 0 & \sin\theta_y & 0 & \cos\theta_y \end{pmatrix}, \\
[R_z(\theta_z)]^\mu_\nu &= \begin{pmatrix} 1 & 0 & 0 & 0 \\ 0 & \cos\theta_z & \sin\theta_z & 0 \\ 0 & -\sin\theta_z & \cos\theta_z & 0 \\ 0 & 0 & 0 & 1 \end{pmatrix},
\end{aligned} \tag{30}$$

Lorentz Boosts (B), mix space and time dimensions. For a rotation mixing time and the x spatial dimension, the dot product is the equation for a hyperbola [25],

$$-c^2t^2 + x^2 = const. \tag{31}$$

From the general hyperbolic trig relationship

$$\cosh^2\phi - \sinh^2\phi = 1. \tag{32}$$

Angle ϕ represents three boosts, which mix space and time.

Preprints (www.preprints.org) | NOT PEER-REVIEWED | Posted: 5 July 2023 doi:10.20944/preprints202307.0325.v1

$$
\begin{aligned}
[B_x(\phi_x)]^\mu_\nu &= \begin{pmatrix} \cosh\phi_x & -\sinh\phi_x & 0 & 0 \\ -\sinh\phi_x & \cosh\phi_x & 0 & 0 \\ 0 & 0 & 1 & 0 \\ 0 & 0 & 0 & 1 \end{pmatrix}, \\
[B_y(\phi_y)]^\mu_\nu &= \begin{pmatrix} \cosh\phi_y & 0 & -\sinh\phi_y & 0 \\ 0 & 1 & 0 & 0 \\ -\sinh\phi_y & 0 & \cosh\phi_y & 0 \\ 0 & 0 & 0 & 1 \end{pmatrix}, \\
[B_z(\phi_z)]^\mu_\nu &= \begin{pmatrix} \cosh\phi_z & 0 & 0 & -\sinh\phi_z \\ 0 & 1 & 0 & 0 \\ 0 & 0 & 1 & 0 \\ -\sinh\phi_z & 0 & 0 & \cosh\phi_z \end{pmatrix}.
\end{aligned} \tag{33}
$$

To clarify the meaning of ϕ.

$$\cosh\,\phi = \gamma \tag{34}$$

and

$$\tanh\,\phi = \beta, \tag{35}$$

so $\sinh\,\phi = \beta\gamma$. We can therefore write the transformation

$$\Lambda^\mu_v = \begin{pmatrix} \cosh\,\phi & -\sinh\,\phi & 0 \\ -\sinh\,\phi & \cosh\,\phi & 0 \\ 0 & 0 & 1 \end{pmatrix}, \tag{36}$$

as

$$\Lambda^\mu_v = \begin{pmatrix} \gamma & -\beta\gamma & 0 \\ -\beta\gamma & \gamma & 0 \\ 0 & 0 & 1 \end{pmatrix} \tag{37}$$

and rewrite Eq.32 as

$$\gamma^2 - \beta^2\gamma^2 = 1 \implies \gamma = \frac{1}{\sqrt{1-\beta^2}}, \tag{38}$$

where

$$\beta = \frac{v}{c}. \tag{39}$$

So Eq.36 becomes

$$\Lambda^\mu_\nu = \begin{pmatrix} \frac{1}{\sqrt{1-\frac{v^2}{c^2}}} & -\frac{\frac{v}{c}}{\sqrt{1-\frac{v^2}{c^2}}} & 0 \\ -\frac{\frac{v}{c}}{\sqrt{1-\frac{v^2}{c^2}}} & \frac{1}{\sqrt{1-\frac{v^2}{c^2}}} & 0 \\ 0 & 0 & 1 \end{pmatrix}. \tag{40}$$

To visualise this in an intuitive way, its helpful to consider three separate stages:

1. Transform Euclidean geodesics on a complex plane under Lorentz boosts to generate the equivalent of a "Poincaré disk" (Figure 11), whose hyperbolic geodesics can be represented at varying levels of complexity.

Preprints (www.preprints.org) | NOT PEER-REVIEWED | Posted: 5 July 2023 doi:10.20944/preprints202307.0325.v1

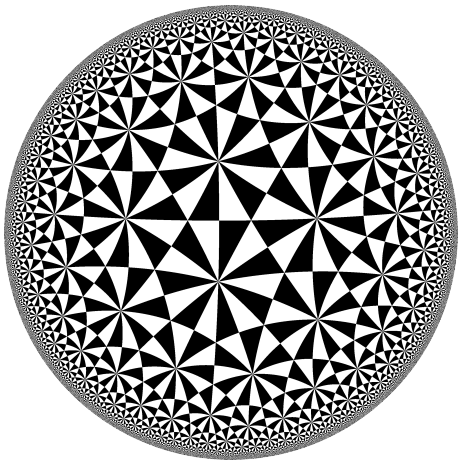

Figure 11. A Poincaré hyperbolic disk.

2. Substitute the Poincaré disc with an approximation of a static, 2D torus, constructed from a set of hyperbolic geodesics to create what might be termed a "Poincaré hyperbolic torus".
3. A final step in the visualisation would be to represent an infinite set of geodesics associated with the dynamic, fluid nature of the recirculating torus under rotation at relativistic velocities. However, even the most detailed set of geodesics that one could technically visualise would represent only a fraction of the geodesics associated with such a complexed fluid structure.

So the Lorentz transformations (Eq's.30 and 33), summarised as

$$\Lambda = e^{iJ.\theta + iK.\phi}, \tag{41}$$

reflect the emergence of a causal dynamic structure from a 4D fractal, fluid space time, which approximates a 2D, hyperbolic spin-1/2 torus, induced by rotational forces as $\dot{\omega} \rightarrow c$.

In addition to a transformation of geodesics under rotation, we also need to accommodate a doubling of the wave function associated with the Lorentz group. Whilst a representation of $SU(2)$ is specified by j (either integer or half-integer), $SO(1,3)$ is specified by two copies of $SU(2)$ (j, j') [25], which reflect a particle and its antiparticle partner in the Dirac equation. This reverts to a single copy of $SU(2)$ at its non-relativistic limit in the Pauli equation.

3.3. The interaction of a torus with the quantum vacuum.

As a toroidal particle rotates, the background media (the quantum vacuum) in which it sits will be continually drawn through its core, then expelled and recirculated, creating a secondary, polarised flux to form a two-component nested torus, analogous with that illustrated in Figure 12.

Preprints (www.preprints.org) | NOT PEER-REVIEWED | Posted: 5 July 2023 doi:10.20944/preprints202307.0325.v1

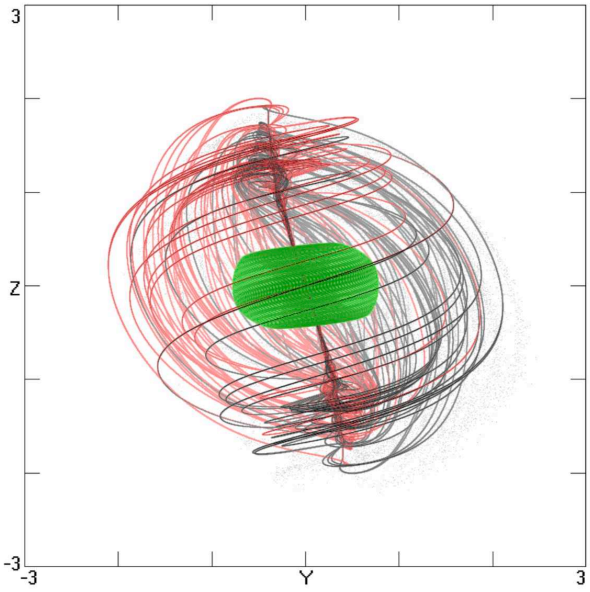

Figure 12. A model of a proton and a secondary, polarised flux (not to scale), creating a charged particle, reproduced from [27].

With a quantum vacuum defined as a field of virtual electrons and photons, it's a small step to identify the outer torus with the permanent magnetic moment (charge) along the axis of a fermion. Such a model offers a very clear insight into the mechanism which underpins the Pauli exclusion principle.

Whilst not to scale, or necessarily of the correct form, we can identify Figure 12 with a simplistic model of a proton with an S_1 orbit, which binds an electron, to produce hydrogen. The model implies a composite, spin-1/2 particle in which an electron is free to pass through its core, traversing parallel hyperbolic flux lines, as it absorbs or emits a quanta of energy (a photon) and changes wavelength.

3.4. A reinterpretation of the macroscopic helix in Figure 8a

.

In earlier comments relating to the double helix structure in Figure 8a [4], it was proposed that the $j = 1/2$ representation (Eq.24) of $SU(2)$ formed the basis of the macroscopic Pauli equation

$$i\widetilde{D}\,\frac{\partial \phi}{\partial t} = \left[\left(i\widetilde{D}\nabla - q\mathbf{A}\right)^2 - q\widetilde{D}\,\mathbf{\text{œ}}.\mathbf{B} + qA_0\right]\phi, \tag{42}$$

which could be used as a basis to describe the structure. Within Eq.42, charge (q), may include an "average charge" on a macroscopic quantum object, such as a protein complex or a stem cell. In this context helicity $\hat{h}$ is generally defined as the projection of spin along the direction of motion:

$$\hat{h} = \mathbf{\Sigma}.\hat{\mathbf{p}} = \mathbf{2S}\hat{\mathbf{p}} = \begin{pmatrix} \sigma & 0 \\ 0 & \sigma \end{pmatrix}.\hat{\mathbf{p}}, \tag{43}$$

with eigenvalues equal to +1 (right-handed) where the spin vector is aligned in the same direction as the momentum vector or -1 (left-handed), where the spin vector is aligned in the opposite direction. Helicity as defined in terms of Eq.43 for a spin $\frac{1}{2}$ particle, represents the product of a two component spinor,

$$\phi = \begin{pmatrix} \psi_1 \\ \psi_2 \end{pmatrix}. \tag{44}$$

Preprints (www.preprints.org) | NOT PEER-REVIEWED | Posted: 5 July 2023 doi:10.20944/preprints202307.0325.v1

However, we now consider an alternative perspective, motivated by a study of vortices in polariton condensates [28]. Images from this work illustrate how coherent quantum vortices can "co-wind", to create a vortex doublet with a structure very similar to that in Figure 8b. Within this context, and that of the more detailed analysis relating to different spin representations in Section 3.1, we conclude that the vortex-like double helix in Figure 8a, more accurately reflects the co-winding of two macroscopic spin-1 vortices.

This reinterpretation also offers a natural fit with the hypothesis that the vortex structure in Figure 8a is underpinned by a coherent macroscopic phonon wave function in the mid infrared range [3], which emerges through a process, which is analogous with Coherent Random Lasing (CRL), within the fractal mesoscale substructure within the vortex. See Section 5 for more detailed discussion on the emergence of CRL

Building on earlier proposals [29,30], a solution to this change of perspective, can be found in $SU(2)$, by substituting the $j = 1/2$ scenario, represented by the 2×2 Pauli matrices in Eq.24, with the spin-1 scenario represented by the 3×3 tau matrices τ_i in Eq.27. The result is a three component wave function

$$|\psi\rangle = \begin{pmatrix} \psi_1 \\ \psi_2 \\ \psi_3 \end{pmatrix}, \tag{45}$$

which we substitute for the two component wave function (Eq.44) within the macroscopic Pauli equation (Eq.42). Within this new context, helicity $\hat{h}$ in Eq.43 is now redefined

$$\hat{h} = \mathbf{\Sigma}.\hat{\mathbf{p}} = \mathbf{3S}\hat{\mathbf{p}} = \begin{pmatrix} \tau & 0 \\ 0 & \tau \end{pmatrix}.\hat{\mathbf{p}}. \tag{46}$$

4. The origin of pointer states and their role in the emergence of quantum particles as causal dynamic structures.

Moving beyond the intrinsic spin of a particle, we examine the concept of "pointer states", whose existence implies some form of hidden, "root-like" substructure, yet to be described as part the internal geometric description of a particle.

If we are to describe these pointer states, we need to understand their origin, nature and role within a wave function, including its transition from a probabilistic to a deterministic classical description. In addition, we need to determine how the new description impacts on a broader understanding of quantum and classical systems.

We begin with a conceptual model in which superfluid helium represents a macroscopic analog of the basic "fabric" of a quantum particle. Within this context the individual magnetic flux generated by each nucleus is shared, the spinning nuclei generating a cascade of eddies/vortices, to create a composite (spin-1/2, spin-1) turbulent field, which defines a BEC. In a decoherence scenario, individual nuclei remain coherent, but localised, thus meeting the definition of pointer states described in Section 1.2.

As a next step we consider the behaviour of a classical fluid in zero gravity space, where a free floating droplet of fluid forms an approximation of a spherical "spin-0" structure, which rotates under the collective angular momentum of individual nuclei. Contrast this with a drop of superfluid helium, allowed to float freely, suspended in zero gravity, below T_c. In such a scenario we would again, initially expect the emergence of a spin-0 structure. However, in the absence of friction (associated with a superfluid), rotational velocity ($\dot{\omega}$) should increase with time. At a critical point in the process of acceleration, we anticipate that centrifugal forces will lead to a transition from a spin-0 structure to a spin-1 (open) vortex, which falls within the definition of a $j = 1$ representation of $SU(2)$ (Eq.27).

From here, we consider a hypothetical process in which a continued increase in $\dot{\omega}$ drives an increase in x and y coordinates and a contraction along the z axis of the vortex. At a critical point in vortex dilation, an increasingly large potential energy, in the form of the basin of attraction (i.e., a

Preprints (www.preprints.org) | NOT PEER-REVIEWED | Posted: 5 July 2023 doi:10.20944/preprints202307.0325.v1

macroscopic quantum potential) created by the vortex core, will attract fluid expelled from the vortex to create a 3D, recirculating torus.

In a final step, as $\dot{\omega} \rightarrow c$, the torus would transform into an approximation of a 2D "Poincaré torus", which falls within our definition of a j=1/2 representation of $SU(2)$ (Eq.24).

The concept offers an insight into a fractal landscape of bifurcating, hyperbolic geodesics within a quantum particle. In this scenario, pointer states (Helium nuclei,) as roots of a finer fractal network, play a key role, generating and maintaining the coherent field that would underpin a macroscopic quantum particle.

Whilst individual nuclei represent pointer states in this scenario, we have yet to describe their equivalence and general applicability of the principle in standard QM.

Within the context of He nuclei representing the roots of a macroscopic quantum particle, it seems a small step to consider a set of nucleons in a larger nuclei in the periodic table, as pointer states, which generate a turbulent field that underpins a coherent nucleus. A cascade of eddies filling the space between nucleons explains the breaking of the internal symmetry of the particle $dt \leftrightarrow -dt$ under reflection [3,17].

The description of the macroscopic spin-0 structure shares some features with the nuclear "liquid-drop model", but with nucleons substituting for nuclei without binding associated with the nuclear force. The proposal also shares with the liquid drop model the limitation that it fails to accommodate the nuclear force and the existence of lines of greater binding energy at certain numbers of protons and neutrons, which forms the basis of the "nuclear shell model".

As in the case for individual nucleons, we can anticipate a breaking of 3D Euclidean symmetry of a large nucleus under rotation. However, it is not clear if this always translates into a spin-1/2 torus, as spin in large nuclear structures is often quoted as an aggregated value of the spin of individual nucleons. Whilst large nuclear structures appear variable, they are generally reported as a broken 3D spherical (e.g., prolate) structures, rather than two dimensional. Although such structures neither confirm or preclude a toroidal structure, a toroidal scenario is supported by NMR measurements on Plutonium 239 (^{239}Pu) [31], which reveal a spin-1/2 nucleus, rotating at $\approx 10^{21}$ times per second. It is currently unclear what specific set of conditions might be responsible for the transition from spin-1 to spin-1/2. However, it seems likely that a particle must either aquire mass as a precursor to the process or as a result of it.

If the concept of nucleons as pointer states is correct, it still leaves an open question relating to a description of an equivalent generators of turbulence (pointer states) which underpin subatomic particles.

Any future model to accommodate the concept of pointer states within a new representation, must at a more simplistic level of interpretation, be naturally reducible to $SU(2)$ and $SO(1,3)$. At the same time one must ultimately be able to describe the smallest level (e.g., quark or subquark structure) at which such an interpretation is valid.

If a subatomic particle such as a proton or quark is represented by a fractal fluid, it suggests some form, of as yet to be defined toroidal field at smaller scale. As summarised in Eq.5, below a critical energy level associated with the quantum force/s within the system (HS), environmental perturbation of the system (HE), is insufficient to induce decoherence at a specific scale of quantisation. This theoretically applies until the minimal scale of quantisation at the Planck scale, where forces dictated by the limits of C reach a maximum. Since no external potential could exceed this force, it forms the bedrock of quantum systems. Wave function collapse at this scale would lead to pure chaos in which quantum forces would cease to exist.

One final point of interest to note from the description above relates to the implication that different structures (spin-0, spin-1 and spin-1/2) may emerge from the same 4D turbulent spacetime geometry as "dynamic causal structures". Whilst this interpretation does not necessarily imply the existence of supersymmetry, it does offer a possible insight into how an underlying principle of shared symmetry might work in practice

Preprints (www.preprints.org) | NOT PEER-REVIEWED | Posted: 5 July 2023 doi:10.20944/preprints202307.0325.v1

5.0. Outstanding questions relating to HTSC materials.

In Section 2.1 we summarised progress in describing the emergence of superconductivity in the p-type cuprates, when charged dopants are incorporated in a thermodynamically driven fractal arrangement. As charge density (ρ) increases, individual charges (ψ_d) begin to interact to generate a charge-induced network of channels ψ_D (Eq.12), illustrated in Figure 3. Above a critical charge density, a critical percolation threshold q_c is crossed. At this point (if $T < T_c$), magnetic flux (magnons) associated with individual charges, begin to interact. Based upon the case studies that have been considered it is proposed that, spinning charges ψ_d (Eq.6) act as pointer states, which generate a turbulent (coherent) magnon condensate ψ_{MG} (Eq.14).

ψ_{MG} preferentially sits in localised wells, such as Figure 1b and the interconnected network of well's and channels (Figure 3). Within this scenario, vortices analogous with that in superfluid Helium (Figure 9b & c) emerge within the magnon condensate in the SC phase ψ_S and pseudo gap ψ_{PG}.

If we consider mechanically induced turbulence in a classical fluid (Section 2.3), we see the transfer of rotational energy throughout the fluid via a cascade of "short-lived", short-range, interacting vortices. By contrast, in a zero viscosity superfluid, there is no dissipation of energy within a vortex. It has the potential to persist indefinitely. However, as seen in Figure 9b & c, energy associated with vortices can bifurcate, with a series of iterations, facilitated by the fractal network of channels (Figure 3), leading to the emergence of a fractal vortex network. In such a scenario the collective correlation energy [1] of vortices is maintained within the fractal network.

When it comes to a description of the mechanism which underpins e-pair formation, we consider a parallel with that of an e-pair traversing the recirculating (spin-1/2) magnetic flux of a nucleus, idealised in Figure 12. In an analogous way, an e-pair can be trapped within spin-1 vortices, which emerge within the magnon condensate. This may explain (at least in part), why e-pair coupling energies are significantly higher than phonon mediated e-pairs in conventional SC, leading to higher values for T_c.

As seen in superfluid He (Figure 9d), when applying a rotational force to the network of vortices in a superfluid, vortices align with that force. An analogous action is anticipated in HTSC. If an electric current is passed through the material, e-pair carrying vortices will align with the electric field, leading to resistance free transport of electrons through the vortex network, creating a superconducting medium.

To clarify additional factors at play in HTSC in more detail, consider two photon vortices rotating at different frequencies. If they collide, the higher energy vortex will disrupt the lower energy vortex, whose energy may then be absorbed in part (or completely) into the dominant vortex, leading to a change in wavelength. Following an iterative series of such interactions in a constrained cavity (which plays the role of a Fabry-Perot resonator), lower energy frequencies will eventually cancel out, to leave a dominant wavelength. We associate such a process with the emergence of a coherent light source, i.e., "lasing". Vortex interactions of this kind, within a localised potential well associated with the PG explains the presence of vortex bound e-pairs ψ_{pg}, which differ from the main superconducting fluid ψ_S. In ψ_S, an analogous process emerges in the fractal network, which supports coherence of a specific wavelength analogous with CRL [1,2]. Within this context, IR frequencies normally associated with e-pair decoherence, will be cancelled out. In other words, the fractal network acts as an insulator against frequencies outside a specific range, which facilitates a higher T_c, compared to conventional SC materials.

At another level, the potential of the vortex network in ψ_S to fractionate (described above) will lead to a lower frequency, lower energy vortex network compared to the PG. This may also explain in part a higher critical temperature in the PG.

A further contribution to higher T_c in the PG arises from the trapping of vortices in potential wells associated with the PG. The localised nature of the well provides an additional level of insulation against spectral perturbation and resistance to decoherence.

Preprints (www.preprints.org) | NOT PEER-REVIEWED | Posted: 5 July 2023 doi:10.20944/preprints202307.0325.v1

6. Conclusions.

6.1. The origins of quantum coherence.

The identification of a quantum signature in turbulent fluids [6], lends support to the hypothesis that a superfluid is underpinned by turbulence generated by a set of interacting pointer states which take the form of a fractal toroidal field. The space between peaks of high energy rotation associated with these pointer states is filled with an interconnected cascade of eddies/vortices, which define a coherent quantum state. Decoherence occurs when spectral density, in the form of an external potential (Eq.3), exceeds the cohesive force of the eddy/vortex cascade, leading to a breakdown of interconnectivity and the localisation of pointer states.

In Section 3.4 we discussed the origin of the magnetic flux (Figure 12) which forms the S_1 orbit of an atom. Taking collective insights from this, superfluid helium (section 2.4) and the p-type cuprates (Section 2.1), a new mechanism for e-pair coupling via magnon vortices in HTSC media is proposed in which a densely packed assembly of charges, acting as pointer states, generate a turbulent magnon superfluid. Vortices which spontaneously emerge as causal dynamic structures within the magnon superfluid bind electron pairs, offering a resistance free highway across the material, to create a superconducting medium.

The concept of macroscopic quantum coherence in HTSC has an analog in biological systems (Section 2.2), where a bosonic condensate, remains coherent in fractal mesoscale networks at room temperatures. Such a system offers a mechanism to transport solar energy (photons) throughout a plant, via a phonon condensate in photosynthetic processes. When we add to this, new insights relating to the emergence of macroscopic vortices emerging within a BEC, then boson condensates associated with fractal media such as cell cytoplasm, offer the potential to facilitate superfluid transport of a range of different "charges" (e.g., electrons, protons, ions and charged biomolecules) across cellular structures, to support processes fundamental to life.

6.2. The Limits of $SU(2)$ and the requirement for a more complexed representation.

Whilst $SU(2)$ is effective in representing a particle such as a proton, it is limited to the extent that it fails to accommodate any form of internal structure which might relate to a description of pointer states and their role in quantum decoherence. It also fails to offer an intuitive insight into intrinsic spin.

In the development of a more detailed description, a number of useful insights have emerged which build upon the basic level of interpretation of $SU(2)$:

- A spin-1/2 fermion is represented by a closed recirculating torus, with its own localised energy and mass, quantised along all three (x,y,z) coordinates. A secondary flux generated by a rotating torus generates the particles magnetic moment (charge).
- A spin-1 boson is represented by an "open vortex", quantised on its x,y coordinates, which facilitates the role of energy transfer.
- A spin-1 boson could also be represented by a closed vortex if the vortex forms a closed loop (or ouroboros). In this scenario, rotation remains along the axis of the vortex, with the winding number (n) impacting on the properties of the system.
- The problem of infinities associated with a point particle is eliminated within the context of a torus or vortex.
- A vortex/torus hypothesis accounts for the probabilistic nature of QM, including spin-1 and spin-1/2 statistics.

Through this process, we identify the complex plane generated by 2D toroidal structures, with the origin of spinors and the complex projective plane ($\mathbb{CP}^1$), which leads to a doubling of the wave function ($\psi_+/\psi-$) and a description in terms of quaternions $\mathbb{H}$ and the Pauli equation. A further doubling of the wave function leads to particles and antiparticles, and a description in terms of bi-quaternions $\mathbb{H}^2$ and the Dirac equation.

$SU(2)$ implies no internal structure, which might reflect pointer states within a particle. Further work is required to consider a more complexed representation, which translates to an intuitive sense that some form of internal structure exists.

Acknowledgments: The authors would like to thank D.P. Lathrop for permission to use the image incorporated in Figure 9 reproduced from [22]. We would also like to thank J. C Sprott for use of the image incorporated in Figure 12, reprinted from [27], with permission from Elsevier.

References

1. Turner. P and Nottale. L. *A New Ab Initio Approach to the Development of High Temperature Superconducting Materials.* Physica C. **515** 15-30 (2015).
2. Turner. P and Nottale. L. *The origins of macroscopic quantum coherence in high temperature super conductivity.* Journal of Superconductivity and Novel Magetism. 29 (12): 3113-3118 (2016).
3. Turner. P and Nottale. L. *The physical principles underpinning self-organization in plants*. Prog. Biophys. Mol. Biol. **123**, 48-73 (2017).
4. Turner. P, Nottale. L, Zhao.J, Pesquet.E. *New insights into the physical processes that underpin cell division and the emergence of different cellular and multicellular structures*. Prog. Biophys. Mol. Biol. **150**, 13-42 (2020).
5. Auffray.C, Noble.D, Nottale.L,Turner *Progress in integrative systems biology, physiology and medicine: towards a scale-relative biology.* European Physical Journal A 56(3) (2020).
6. Nottale. L; Lehner. T. *Turbulence and scale relativity.* Phys. Fluids 31, 105109 (2019)
7. Nottale. L and Célérier. M.N. *Derivation of the postulates of quantum mechanics from the first principles of scale relativity.* J. Phys. A: Math. Theor. 40 (2007) 14471-14498.
8. Nottale. L and Auffray. C. *Scale relativity theory and integrative systems biology: 2. Marcroscopic quantum-type mechanics*. Prog. Biophys. Mol. Biol. **97**, 115-157 (2008).
9. Schlosshauer. M. *The quantum-to-classical transition and decoherence* , arXiv:1404.2635v1 [quant-ph] (2014).
10. Zurek. W.H. Rev. Mod. Phys. **75**, 715 (2003)
11. Joos. E, Zeh. H.D, Kiefer. C, Giulini. D, Kupsch. J, Stamatescu. I.O. *Decoherence and the Appearance of a Classical World in Quantum Theory*. 2nd edn. Springer, New York, (2003)
12. Kubler. O, Zeh. H.D Ann. Phys. (N.Y.) **76**, 405 (1973)
13. Paz. J.P, Habib. S, Zurek. W.H, Phys. Rev. D **47**, 488 (1993)
14. Zurek. W.H. Prog. Theor. Phys. **89**, 281 (1993)
15. Diosi. L, Kiefer. C. Phys. Rev. Lett. **85**, 3552 (2000)
16. Auffray. C and Nottale. L. *Scale relativity theory and integrative systems biology: 1. Founding principles and scale laws*. Prog. Biophys. Mol. Biol. **97**, 79-114 (2008).
17. Nottale. L. Scale Relativity and Fractal Space-time. *A new approach to Unifying Relativity and Quantum Mechanics* (2011). Imperial College Press. ISBN 978-1-84816-650-9.
18. Nottale. L. *Fractal Space-Time and microphysics. Towards a theory of scale relativity* (1993). World Scientific. ISBN 9810208782.
19. Célérier. M.N and Nottale. L. *The Pauli Equation in scale relativity.* J. Phys. A, 39, 12565 (2006) arXiv:quant-ph/0609107v1.
20. Célérier. M.N and Nottale. L. *Dirac Equation in scale relativity.* J. Phys. A 37, 931-955 (2004). arXiv:hep-th/0112213.
21. Vincent , A., Meneguzzi, M. The spatial structure and statistical properties of homogeneous turbulence. J. Fluid Mech. vol. 225, 1-20 (1991).
22. Bewely G.P., Lathrop. D.P., Sreenivasan. K. R. Superfluid helium. Visualization of quantized vortices. NATURE. Vol 44.1 p 588. June 2006
23. Kyriakos.A.G. *Non-linear field theory III. Geometrical illustration of the electromagnetic representation of Dirac's electron theory.* arXiv:quant-ph/0407071 (2004).
24. Johnson. D. *The Spin Torus Energy Model and Electricity*. Open Journal of Applied Sciences, 2019, 9, 451-479. www.scirp.org/journal/ojapps
25. Robinson. R. *Symmetry and the Standard Model Mathematics and Particle Physics*. Springer, ISBN 978-1-4419-8266-7 (2011).

26. Nottale. L; Lehner. T. *Numerical simulation of a macro-quantum experiment:oscillating wave packet.* Int. J. Mod. Phys. C23 (5), 1250035.
27. Sprott. J. C. *A dynamical system with a strange attractor and invariant tori.*. Phys. Lett. A 378, 1361-1363 (2014)
28. Dominici. L, Carretero-Gonzalez. R, Gianfrate. A, Cuevas-Maraver. J, Rodrigues. A.S, Frantzeskakis. D.J, Lerario. G, Ballarini. D, De Giorgi. M, Gigli. G, Kevrekidis. P.G, Sanvitto. D. *Interactions and scattering of quantum vortices in a polariton condensate.* Nature Communications. 9:1467 (2018).
29. Oppenheimer. J.R. *Note on light quanta and the electromagnetic field.* Physical Review. Vol 38, 725-746 (1931).
30. Mohr. P.J. *Solutions of the Maxwell equations and photon wave functions.* Annals of Physics **325**, 607-663 (2010). http://www.nist.gov/pml/div684/fcdc/upload/preprint.pdf.
31. H. Yasuoka, G. Koutroulakis, H. Chudo, S. Richmond, D. K. Veirs, A. I. Smith, E. D. Bauer, J. D. Thompson, G. D. Jarvinen,1 D. L. Clark. *Observation of 239Pu Nuclear Magnetic Resonance*. Science 336(6083):901-4 (2012).